THE JOURNAL OF PHYSICAL CHEMISTRY A

Article

pubs.acs.org/JPCA

Theoretical and Experimental Studies of the Dechlorination Mechanism of Carbon Tetrachloride on a Vivianite Ferrous Phosphate Surface

Keonghee Jeon,[†,⊥] Nara Lee,[‡,⊥] Sungjun Bae,[§] William A. Goddard, III,[∥] Hyungjun Kim,*[,†] and Woojin Lee*[,‡]

[†]Graduate School of Energy, Environment, Water, and Sustainability (EEWS), Korea Advanced Institute of Science and Technology (KAIST), Yuseong-gu, Daejeon 305-701, Korea

[‡]Department of Civil and Environmental Engineering, Korea Advanced Institute of Science and Technology (KAIST), 291 Daehak-ro, Yuseong-gu, Daejeon 305-701, Korea

[§]École Nationale Supérieure de Chimie de Rennes, UMR CNRS 6226, 11 Allée de Beaulieu, 35708 Rennes Cedex 7, France

[∥]Materials and Process Simulation Center, Beckman Institute, California Institute of Technology, Pasadena, California 91125, United States

Supporting Information

ABSTRACT: Chlorinated organics are the principal and most frequently found contaminants in soil and groundwater, generating significant environmental problems. Over the past several decades, Fe-containing minerals naturally occurring in aquatic and terrestrial environments have been used as natural electron donors, which can effectively dechlorinate a variety of chlorinated organics. However, a full understanding of the reaction mechanism of the dechlorination pathway cannot be obtained by experimental investigations alone, due to the immeasurability of chemical species formed over a short reaction time. In this report, we describe experiments and density functional theory (DFT) calculations carried out to investigate the complex reduction pathway of carbon tetrachloride (CT) on a vivianite ($Fe^{II}_3(PO_4)_2{\cdot}8H_2O$) surface. Our results indicate that chloroform ($HCCl_3$) and formate are the primary transformation products. The experimental results reveal that the reduction kinetics of CCl_4 can be dramatically accelerated as the pH is increased from 3 to 11. On the basis of the DFT calculations, we found that $HCCl_3$ can be formed by $^{\bullet}CCl_3$ and $:CCl_3^{-}$* on a deprotonated vivianite surface (an adsorbate on vivianite is denoted using an asterisk). In addition, $:CCl_3^{-}$* can be nonreductively dechlorinated to form $:CCl_2$* followed by sequential nucleophilic attack by OH^{-}*, resulting in the formation of :CCl(OH)* and $:C(OH)_2$*, which are responsible for production of CO and formate, respectively. The results obtained from this study can facilitate the modeling of systems of other halogenated species and minerals, which will provide fundamental insight into their corresponding reaction mechanisms.

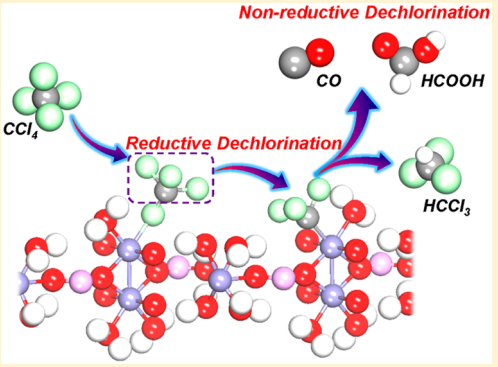

I. INTRODUCTION

Chlorinated organics are widely used for industrial purposes[1] and are commonly found as principle contaminants in soil and groundwater.[2−4] It is well-known that most chlorinated organics are highly toxic and are persistent and widely spread in natural environments due to their limited water solubility and downward migration.[3] Because of their harmful effects, maximum concentrations of chlorinated organics in water used for various purposes have been set by the World Health Organization; however, they have still been detected in a third of US hazardous waste sites owing to past inappropriate disposal practices.[5] As a result, remediation technologies that can treat a variety of chlorinated organics have been developed extensively over the past few decades. Among these, soil and soil minerals, particularly Fe-containing minerals existing in natural environments, have attracted attention as natural attenuators, which are utilized as efficient electron donors under iron-reducing environments.[4,6,7] Indeed, a variety of Fe-containing minerals have shown a remarkable reduction capacity toward various chlorinated organics. For example, Lee and Batchelor reported the reductive degradation of chlorinated ethylenes (tetrachloroethylene (PCE), trichloroethylene (TCE), *cis*-dichloroethylene, and vinyl chloride) by pyrite, magnetite, and green rust.[8] Additionally, Amir and Lee[9] demonstrated an enhanced reactivity of nanomackinwite for PCE, and Choi et al.[10] reported the reductive dechlorination of

Received: February 25, 2015
Revised: April 29, 2015
Published: April 29, 2015

DOI: 10.1021/acs.jpca.5b01885
J. Phys. Chem. A 2015, 119, 5714−5722

carbon tetrachloride (CT) and 1,1,1-trichloroethane by iron sulfide.

Recently, the monoclinic octa-hydrated ferrous phosphate vivianite ($Fe^{II}_3(PO_4)_2{\cdot}8H_2O$) has been rehighlighted as a potential reactive Fe-containing mineral due to its adsorption capacity, leading to the immobilization of cobalt, nickel,[11] strontium,[12] and arsenic,[13] as well as its reduction capacity, leading to the reduction of oxidized uranium[14] and CCl_4[4]. In our previous study, the transformation of CCl_4 into CO and formate by vivianite and surface-stabilized carbene complexes, respectively, was suggested as the main reaction process.[4] However, the difficult experimental detection of the intermediates has always prevented a full understanding of the dechlorination pathway due to the extremely short reaction time, low concentration of products, and immeasurability of chemical species. Therefore, a novel approach should be carried out to investigate the complex surface reactions of CCl_4 and its intermediates with a vivianite surface.

Now regarded as an indispensable supplement to experiments, density functional theory (DFT) calculations are being used in a wide range of applications to aid in the interpretation of experimental observations and in the investigation of the full atomistic details of reaction pathways based on accurate quantum mechanical energetics.[15−18] The most beneficial feature of DFT studies is that they provide relative energies of intermediate states based on first-principles quantum mechanics, which can be unbiasedly utilized to determine the feasibilities of possible reaction pathways. Although several previous studies have investigated Fe-containing minerals using DFT calculations to understand the bulk and surface structures of hematite,[19] magnetite,[20] siderite,[21] and vivianite.[22] Also, electrocatalytic activity[23] and water oxidation[24] on Fe-containing minerals were studied using DFT calculation. However, to the best of our knowledge there have been no DFT studies on the catalytic activity between vivianite and chlorinated compounds.

In this paper, we describe a combined experimental and DFT study carried out to examine the reductive dechlorination mechanisms of CCl_4 on a vivianite surface. We experimentally studied the reductive dechlorination of CCl_4 by vivianite, the effect of pH on the CCl_4 degradation, and the intermediate and final product distributions during the dechlorination process. Using DFT, we investigated the energetics of possible intermediate states and of the dominant reaction mechanism, which explain the experimentally observed results.

II. METHODS

Chemicals. The chlorinated organics used in this study, CCl_4 (≥99.5%), chloroform ($HCCl_3$) (≥99.5%), dichloromethane (CH_2Cl_2) (≥99.5%), and methyl chloride (CH_3Cl) (≥99.9%), were all purchased from Sigma-Aldrich. Ammonium ferrous sulfate hexahydrate (99%, Sigma-Aldrich), sodium acetate anhydrous (>99%, Aldrich), and sodium phosphate dibasic anhydrous (99%, Junsei) were used for the synthesis of vivianite. Hexane (99.9%, Merck) and methanol (≥99.9%, Sigma-Aldrich) were used as an extractant for the chlorinated organics and as a solvent for the preparation of stock solutions, respectively. A SCOTTY gas mixture (1.01% of methane (CH_4), carbon monoxide (CO), carbon dioxide (CO_2), ethane, acetylene, and ethylene in N_2, Supelco) was used to analyze the nonchlorinated transformation products. Formic acid (≥95%, Sigma-Aldrich) and sodium chloride (≥99%, Sigma-Aldrich) were used for the analysis of formate and chloride ion, respectively.

Deaerated deionized water (DDW) was prepared by purging ultrapure water (18 MΩ·cm) with N_2 for 4 h, and was subsequently stored under anaerobic conditions. The organic buffers used in this study were citric acid monohydrate and trisodium citrate dihydrate (for pH 3 and 5), 1,4-piperazinediethanesulfonic acid (PIPES, for pH 7), 2-(cyclohexylamino)ethanesulfonic acid (CHES, for pH 9) and 3-(cyclohexylamino)-1-propanesulfonic acid (CAPS, for pH 11). All of the buffers (0.03 M) were adjusted to the exact required pH using sodium hydroxide aqueous solution (1 M). Unless otherwise stated, all of the chemicals used in this study were used as received without further treatment.

Synthesis of Vivianite. Vivianite was synthesized by following the method previously described.[21] An aqueous solution of $Fe(NH_4)_2SO_4{\cdot}6H_2O$ (80 g/L) and a solution containing CH_3OONa (13.33 g/L) and Na_2HPO_4 (66.67 g/L) were mixed under continuous stirring for 2 days in an anaerobic chamber (Coy Laboratory Products Inc.). The bluish-gray precipitate was continuously washed with DDW to remove remnant iron species during its synthesis. The iron contents in the aqueous phase were monitored after each washing process until the supernatant solution was free of iron. The washed vivianite was then centrifuged and dried under anaerobic conditions, after which it was analyzed by X-ray diffraction (XRD). The XRD results of the synthesized vivianite agreed well with the corresponding Joint Committee on Powder Diffraction Standards (JCPDS) diffraction data.

Experimental Procedures. Batch experiments were conducted to investigate the degradation kinetics of CCl_4 by vivianite. Borosilicate glass vials (23.4 mL) sealed with a three-layered septum system (PTFE film, PTFE film-lined rubber septum, and lead foil) were used as batch reactors. The buffer solutions (23.3 mL), prepared using a previously described method,[4] were transferred to vials each containing the same amounts of vivianite (0.234 g). Each vial was spiked using a gastight syringe (Hamilton) with 100 μL of CCl_4 stock solution (23.4 mM) prepared in methanol, resulting in an initial CCl_4 concentration of 0.1 mM. The vials were then taken out from the anaerobic chamber and placed on a tumbler (7 rpm) for vertical mixing. To investigate the effect of pH on the dechlorination of CCl_4 by vivianite, five different buffer solutions (pH 3, 5, 7, 9, and 11) were used. Controls (buffer solutions without vivianite) at the different pHs were also prepared to evaluate potential losses during the reaction. All of the experiments in this research were conducted in duplicate at 26 ± 0.5 °C.

Analytical Procedures. CCl_4 and the other chlorinated transformation products were quantified using a gas chromatograph (GC) equipped with electron capture detector (ECD, GC-2010 Plus, Shimadzu, Co.) and HP-5 column. At each sampling time, the vials were centrifuged at 3000 rpm for 5 min and a 100 μL portion of the supernatant was transferred to a 2 mL GC vial containing 0.9 mL of hexane with an internal standard (i.e., 0.25 mM 1,2-dibromopropane). The GC vials were shaken at 150 rpm using an orbital shaker for 1 h to extract the chlorinated organics, and the extractant (1 μL) was automatically injected into the injector (200 °C) with a split ratio of 30:1. The temperatures of the detector and oven were kept constant at 230 and 100 °C, respectively.

The nonchlorinated hydrocarbon transformation products were analyzed using a GC equipped with a flame ionization

DOI: 10.1021/acs.jpca.5b01885
J. Phys. Chem. A 2015, 119, 5714−5722

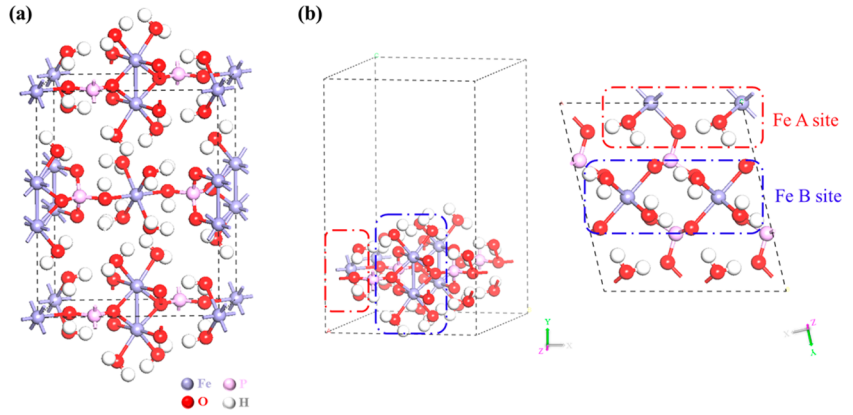

Figure 1. (a) Optimized structure of bulk vivianite using DFT, and (b) (010) surface slab model of vivianite (left panel). Two distinct Fe^{II} sites exist on the surface, which are denoted as Fe A site and Fe B site (see top view of the surface slab model shown in the right panel).

detector (FID, YL6500GC, Young Lin Instrument Co.) and a GS-alumina column. After centrifugation of the vials prior to each sampling time, the supernatants (10 mL) were transferred to amber glass vials (23.4 mL) and allowed to stand for 1 h to allow the various chemicals in the gas and liquid phases to equilibrate. A 100 μL sample of the gas was then taken out from the vials and injected into the GC injection port. The temperatures of the detector and injector were set to 200 and 220 °C, respectively, and the oven temperature was set to 45 °C for 1 min and subsequently increased to 155 °C at a rate of 10 °C/min.

CO was measured by GC with thermal conductivity detector (GC-TCD, HP 5890, Hewlett-Packard) and Molecular sieve 5A column. The temperatures of the injector, detector, and oven were kept constant at 180, 200, and 160 °C, respectively. The analytical procedures were same as previously described for GC-FID analysis.

Formate was analyzed by high-performance liquid chromatograph (HPLC, SDV30PLUS, Younglin) equipped with C18 packed column (Shiseido). The mobile phase was prepared by mixing DDW with phosphoric acid (0.1%) and acetonitrile (2.5%) and 210 nm of wavelength was used for detection of formate at 1.0 mL/min flow rate.

Computational Details. We carried out spin-polarized DFT calculations using the Vienna ab initio simulation package (VASP) code[25] with a plane-wave basis set. The exchange and correlation (xc) energy was described by the functional form of Perdew, Burke, and Ernzerhof (PBE).[26] It is of noted that PBE functional is regarded to be reliable in predicting equilibrium properties such as lattice parameters of the vivianite structure although it underestimates the band gap due to the self-interaction error.[22] The vivianite (010) surface was cleaved by a (2 × 1 × 1) periodic cell with a 15 Å vacuum slab. A (2 × 2 × 1) k-point grid and a plane-wave basis set with a kinetic energy cutoff of 450 eV were employed. To describe the solvation phase, we used an implicit Poisson−Boltzmann (PB) solvation method[27] as implemented in the VASP program, employing a dielectric constant of 80 for water and neglecting the contribution of the cavitation energy.

The DFT optimized bulk structure for vivianite is shown in Figure 1a. The simulation cell consists of three iron atoms, two phosphate groups, and eight water molecules that coordinate to the iron atoms. The optimized cell parameters are a = 9.99 Å, b = 12.84 Å, c = 4.77 Å, and β = 103.82°, which agree well with the experimental values of a = 10.021 Å, b = 13.441 Å, c = 4.721 Å, and β = 102.84°.[28]

The vivianite has a layered structure in which stacking occurs along the b-direction, where relatively weak hydrogen bonds between the H_2O ligands connect each layer. Therefore, the most stable surface of vivianite is the (010) surface,[29] which is shown in Figure 1b. On the surface, two distinct types of iron centers are exposed: (1) Fe A sites, which are iron atoms coordinated by two H_2O molecules, four phosphate oxygen atoms, and one iron atom, and (2) Fe B sites, which are iron atoms coordinated by four H_2O molecules and two phosphate oxygen atoms. We found that the energy states near the Fermi level are mostly contributed by Fe 3d states with negligible contribution by phosphate groups (Figure S1, Supporting Information). Since the reduction chemistry is dominated by the valence states, we think that the primary role of phosphate group is to structurally stabilize the ferrous ion within the crystal surface where the CCl_4 uptakes an electron.

In our calculations, we fully relaxed the positions of the nuclei in the one-layer slab model of vivianite with the (010) surface, which was employed to investigate the CCl_4 dechlorination pathway (the a, c, and β cell parameters were fixed as their bulk values, which were optimized using DFT). In addition, we assumed that the sequential transformations of chemical species were occurred on vicinal Fe centers, not only for the brevity of our calculations with limited size of the simulation cells but also for considering that the reaction intermediate radicals (e.g., $^{\bullet}CCl_3$) would have not enough lifetime to migrate to non-neighboring Fe centers. However, we note that there could be a possibility that the reactions undergo at distant Fe centers, which might slightly change the reaction energetics.

III. RESULTS AND DISCUSSION

Experimental Results on the Reductive Degradation of CCl_4 by Vivianite. Figure 2 shows the dechlorination kinetics of CCl_4 by vivianite at pH 7. The control solutions without vivianite showed no significant change in the CCl_4 concentration over a period of 40 d, indicating that CCl_4 loss by sorption in the batch reactor or volatilization during the sampling process was not significant in this study. In contrast with the control solutions, approximately 90.3% of the initial CCl_4 was removed by vivianite in 40 d. Over the course of the CCl_4 reduction, $HCCl_3$ and formate gradually increased, finally reaching levels of 0.051 and 0.016 mM at the last sampling

DOI: 10.1021/acs.jpca.5b01885
J. Phys. Chem. A 2015, 119, 5714−5722

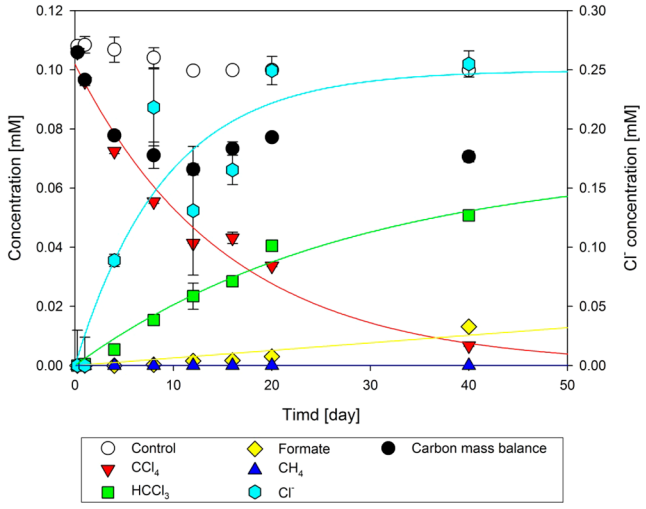

Figure 2. Degradation of CCl_4 and the formation of products ($HCCl_3$, formate, methane, and chloride) at pH 7.

time, while a negligible amount of methane was detected during the reaction. CH_2Cl_2 and CH_3Cl were not detected in this study. We also observed a continuous increase (to ~0.25 mM) in the amount of chlorine ion in aqueous solution, with 97.6% chlorine mass balance measured at the last sampling time. The total carbon mass fluctuated from 62.6–91.2% during the reaction, indicating that some of the nonchlorinated intermediates may be (1) volatilized during the sampling process, (2) sorbed on the mineral surface, and (3) undetected by the analytical methods used in this study. The formation of $HCCl_3$ and formate accompanying the CCl_4 degradation implies that both the hydrogenolysis and the carbene hydrolysis pathways may have occurred simultaneously.[30,31] More details regarding the formation of $HCCl_3$ and formate, as well as of the nonchlorinated intermediates on the vivianite surface during the CCl_4 degradation, will be discussed in the next section.

Figure 3a shows the effect of pH (pH 3, 5, 7, 9, and 11) on the reduction kinetics of CCl_4 by vivianite. The dechlorination kinetics of CCl_4 seem to accelerate as the pH is increased from 3 to 11. All of the degradation kinetics of CCl_4 by vivianite can be described by the pseudo-first-order kinetic model.[30] The highest observed rate constant was obtained at pH 11 (0.174 ± 0.0019 d^{-1}), followed by pH 9 (0.0693 ± 0.0059 d^{-1}), pH 7 (0.0651 ± 0.0064 d^{-1}), pH 5 (0.0406 ± 0.0074 d^{-1}), and pH 3 (0.0116 ± 0.0022 d^{-1}) (Figure 3b and Table S1). The enhanced CCl_4 degradation at higher pH values may be due to the greater electron density caused by deprotonation of the active sites under basic conditions, similar to the case of magnetite.[30] Because the point of zero charge of vivianite has been known as pH ~5.3,[13] the basic water will donate more hydroxide groups and the surface will be negatively charged above this point.[13,32] Therefore, more deprotonated surface sites can be generated by an increase of the pH, resulting in the acceleration of CCl_4 dechlorination by vivianite. More details regarding the importance of OH^{-}* during the reductive degradation of CCl_4 will be discussed in the next section. Adsorbed hydrogen and hydroxide ions on the mineral surface can also catalyze Fe separation from the reactive site.[13] At low pH, extensive protonation at the surface can weaken structural iron bonds due to polarization and finally detach the reactive iron species,[33] resulting in an exponential increase in the dissolution rate of vivianite as a function of the acidity.[13] Thus, the results from this study indicate that basic condition can lead to the preservation of reactive iron species on the vivianite surface, which is favorable for the dechlorination of CCl_4 by vivianite. The rate constants for the productions of $HCCl_3$, formate, and chloride ion were fitted using a pseudo-first-order kinetic model (Figure 3c and Table S1). The rate constants increase with increasing pH, which is similar to the kinetics of CCl_4 degradation in various pHs (Figure 3b). This may also be attributed to both the surface deprotonation and the changes in iron solubility, as described above.

DFT Energetics and the CCl_4 Dechlorination Mechanism. The dechlorination of CCl_4 involves a reduction process coupled with the oxidation of the Fe^{II} of vivianite, which is consumed into Fe^{III}. Initiation of the reaction therefore requires the generation of an undercoordinated Fe^{II} site, i.e., the reactive site on the mineral surface,[35] where the CCl_4 can bind and acquire an electron from the Fe center. We calculated the surface activation energy required to expose an Fe^{II} center by removing one coordinating water molecule (Figure 4a). The DFT-calculated water desorption energy on the Fe A site is

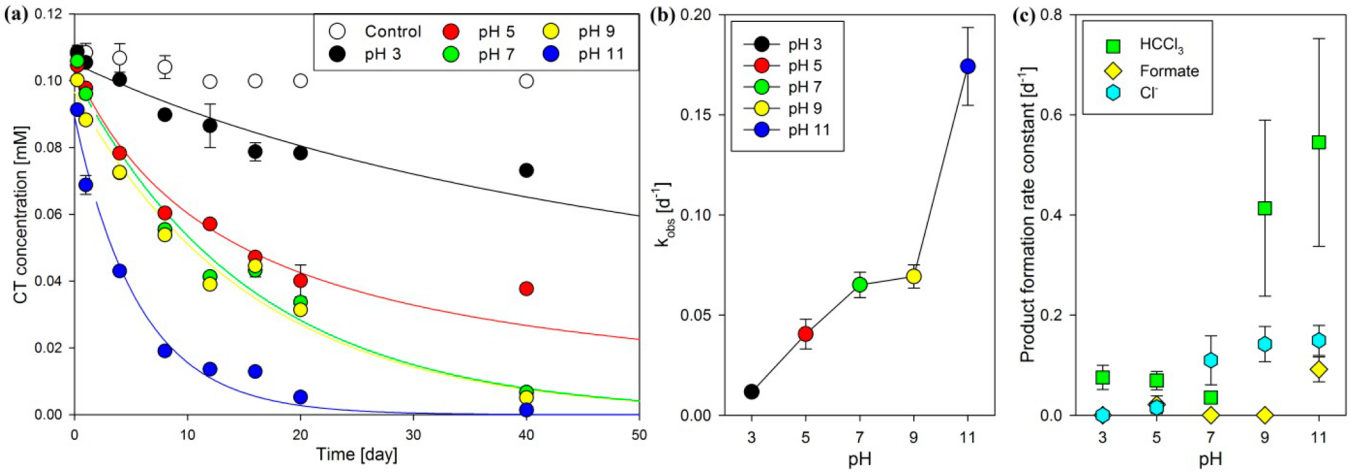

Figure 3. (a) Effect of the suspension pH (3–11) on the CCl_4 degradation kinetics with vivianite. The initial concentration of CCl_4 was 0.1 mM and standard deviations obtained from duplicate measurements are indicated as the error bars. (b) Change in the observed kinetic constants for the reductive dechlorination of CCl_4. (c) Product formation rate constants for $HCCl_3$, formate, and chloride ion as a function of pH.

DOI: 10.1021/acs.jpca.5b01885
J. Phys. Chem. A 2015, 119, 5714–5722

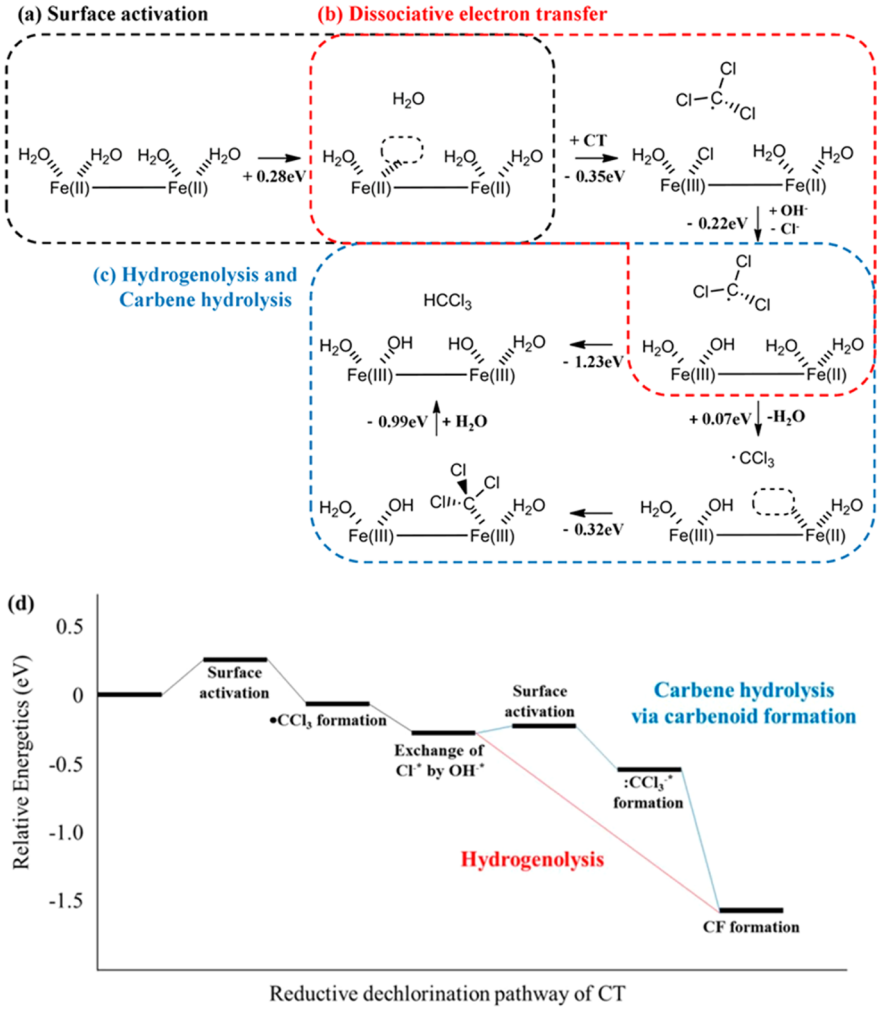

Figure 4. (a) Surface activation step, requiring 0.28 eV energy to remove one water molecule coordinating the surface Fe^{II}. (b) Dissociative electron transfer (diss-ET) from CCl_4 to Fe^{II} of the vivianite surface, yielding one chlorine remaining on the surface and a trichloromethyl radical ($^{\bullet}CCl_3$). This process is 0.57 eV downhill. (c) After diss-ET, the unstable $^{\bullet}CCl_3$ uptakes either a hydrogen atom to form a molecule of chloroform ($HCCl_3$) (hydrogenolysis pathway; 1.23 eV downhill) or an electron while adsorbed on the surface to form a carbenoid ($:CCl_3^{-}$*), followed by a proton uptake (carbene hydrolysis pathway via carbenoid formation). To form $:CCl_3^{-}$*, the surface Fe^{II} must be activated (0.07 eV uphill), and $^{\bullet}CCl_3$ is adsorbed while oxidizing the Fe center (0.32 eV downhill). Subsequent $HCCl_3$ formation from CCl_3^{-}* is another exothermic process by 0.99 eV. (d) Relative energy diagram for the overall dechlorination of CCl_4 to form $HCCl_3$.

0.35 eV and that on the Fe B site is 0.28 eV. We note that the desorption of water involves an entropic gain, facilitating the water desorption, because the liquid water molecule has more degrees of freedom of which extent can be estimated as ∼0.1 eV considering the entropy of water (70 J/mol/K) and the entropy of ice (41 J/mol/K).

We investigated the binding affinities of the chlorinated compounds at the reactive site generated on the Fe B site, which has the lower water desorption energy. When CCl_4 is placed near the Fe^{II} in the initial structure of the DFT calculation, it spontaneously decomposes into trichloromethyl radical ($^{\bullet}CCl_3$), and after performing the geometry optimization steps, one Cl^- ion is observed to be left behind on the Fe site. In other words, a dissociate electron transfer step (diss-ET) takes place. Our DFT results showed that the diss-ET energy of CCl_4 is 0.35 eV downhill with a negligible reaction barrier (Figure 4b). We then determined that the adsorbed Cl^- is replaced with OH^- with a downhill reaction energy of 0.22 eV (evaluated following Scheme S1), which supports the experimental result demonstrating a significant increase in the chlorine ion concentration in the aqueous phase. This is also consistent with a previous discussion suggesting that the reductive deformation of CCl_4 by Fe-containing minerals[4,31,35−38] is initiated by the first electron transfer and is followed by bond cleavage between carbon and chloride.[39,40]

After the diss-ET step, hydrolysis of CCl_4 can occur in two ways: trichloromethyl radical ($^{\bullet}CCl_3$) can be transformed to chloroform ($HCCl_3$) by abstracting hydrogen (hydrogenolysis),[41] or it can be further reduced to form trichlorocarbanion as a surface-stabilized form ($:CCl_3^{-}$*) that is released as a form of $HCCl_3$ by abstracting a proton (carbenoid formation).[42] We have investigated the DFT energetics required for these two pathways.

For the hydrogenolysis pathway, we calculated the energetics associated with the uptake of one hydrogen atom by $^{\bullet}CCl_3$ from the water molecule coordinating Fe^{II} (assumed to be the nearest Fe B site in our calculations), accompanied by the oxidization of Fe^{II}. This yields $HCCl_3$ and two oxidized Fe^{III} centers coordinated to OH^- on the surface, resulting in a net change in energy calculated as 1.23 eV downhill (Figure 4c).

DOI: 10.1021/acs.jpca.5b01885
J. Phys. Chem. A 2015, 119, 5714−5722

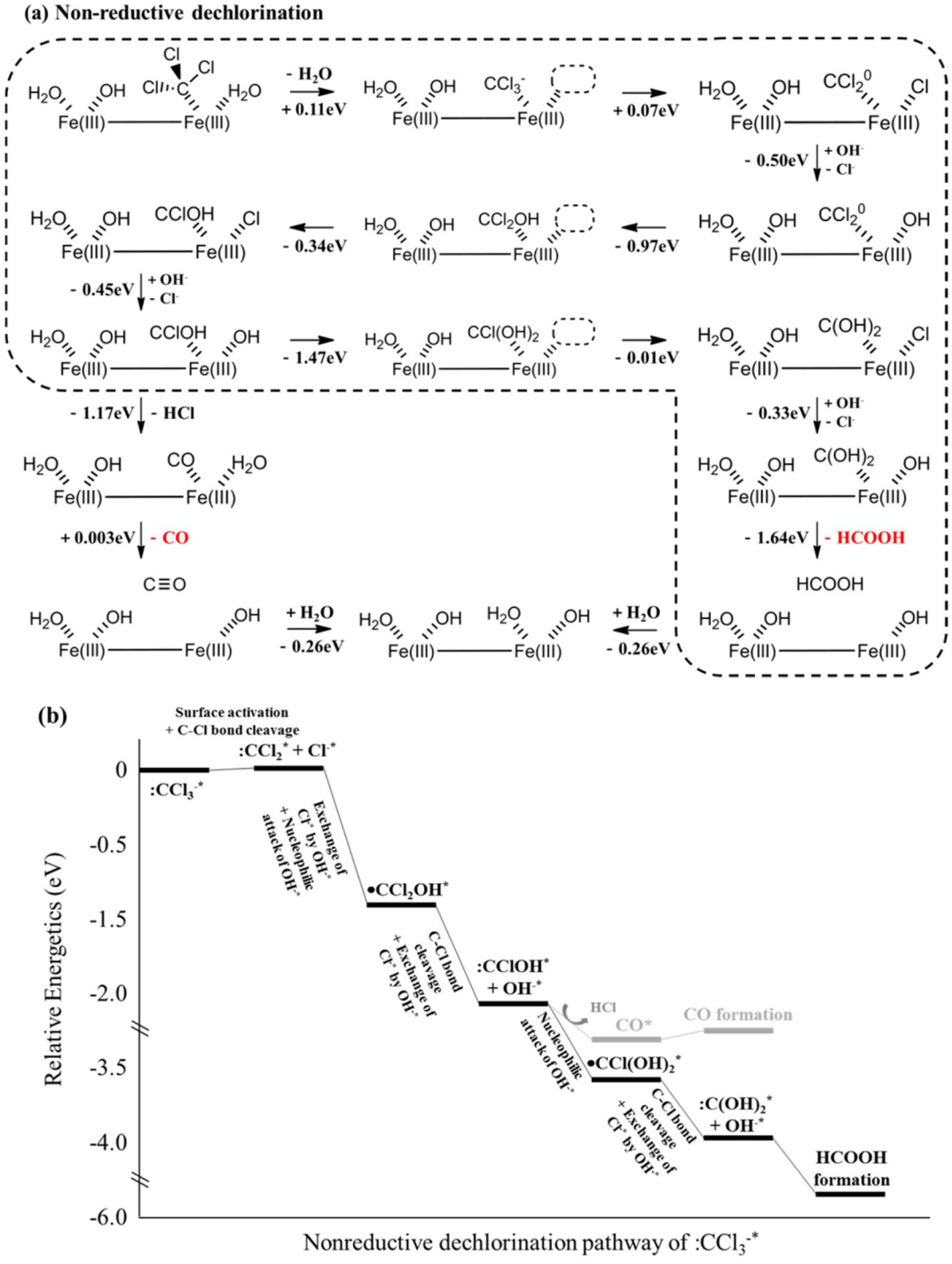

Figure 5. (a) Nonreductive dechlorination (nr-deCl) of $:CCl_3^-$*. When one water molecule is desorbed from the surface (0.11 eV), $:CCl_3^-$* can be decomposed into dichlorocarbene ($:CCl_2$*) and Cl^-* on the surface (0.07 eV uphill). Cl^-* is then exchanged with OH^- in the solution phase (0.50 eV downhill), where OH^-* undergoes a nucleophilic attack on $:CCl_2$* to form $:CCl_2OH$*. The subsequent additional C−Cl bond cleavage is an exothermic process by 0.34 eV, which yields CClOH* and Cl^-*. If an electron rearrangement takes place, leaving behind H^+ and Cl^-, :CClOH* is converted to CO* (1.17 eV downhill), which can be easily released from the surface (0.003 eV uphill). Otherwise, OH^-* (which is replaced with Cl^-* in a 0.45 eV downhill process) participates in a nucleophilic attack on :CClOH*, yielding $:CCl(OH)_2^-$* (1.47 eV downhill process). An additional C−Cl bond cleavage of $:CCl(OH)_2^-$* yields $C(OH)_2$* and Cl^-* (0.01 eV downhill), where $C(OH)_2$* is desorbed from the surface while proton rearrangement yields the formic acid (HCOOH). (b) Relative energy diagram for the overall nonreductive dechlorination of $:CCl_3^-$* to form either CO or HCOOH.

For the carbenoid formation pathway, we considered the following sequential reactions: (1) One additional water molecule desorbs from the Fe^{II} site of the surface to expose the second active site of Fe^{II} (assumed to be the adjacent Fe B site in our calculations). (2) $^{\bullet}CCl_3$ adsorbs to that vacancy site of Fe^{II}, leading to immediate oxidization of the Fe^{II} center into an Fe^{III} center, while $^{\bullet}CCl_3$ acquires another electron to form an adsorbed trichlorocarbanion, i.e., a carbenoid ($:CCl_3^-$*). (3) $:CCl_3^-$* desorbs from the surface while associating with one proton in the solution phase, yielding a molecule of $HCCl_3$,

DOI: 10.1021/acs.jpca.5b01885
J. Phys. Chem. A 2015, 119, 5714−5722

while the resulting OH^- stabilizes the oxidized Fe^{III} center. As summarized in Figure 4c, the DFT energetics of this pathway are (1) 0.07 eV uphill for the second water desorption, (2) 0.32 eV downhill for the adsorption of $^{\bullet}CCl_3$ to form $:CCl_3^-$*, and (3) 0.99 eV downhill for the final $HCCl_3$ formation. This implies that both the hydrogenolysis and carbenoid formation pathways are responsible for the $HCCl_3$ production.

By repeating either of the hydrogenolysis or carbenoid formation pathways, CH_2Cl_2, CH_3Cl, or methane can be formed, as has been observed in other Fe-containing mineral systems.[31] However, the DFT energy for the diss-ET step to $HCCl_3$ was calculated as 0.37 eV uphill (Figure S2), indicating that further reduction is energetically unfavorable. This supports our experimental results, which show that no significant amount of methane was generated and that CH_2Cl_2 and CH_3Cl were also not detected. It also explains why the dechlorination of $HCCl_3$ hardly occurs in the presence of vivianite.[43]

Instead of further sequential reductive dechlorinations, we considered a nonreductive dechlorination (nr-deCl) pathway of $HCCl_3$. The chemical equilibrium of $HCCl_3$ can be considered as follows:

$$HCCl_3(aq) \rightleftharpoons :CCl_3^-(aq) + H^+(aq) \quad K_a$$

$$:CCl_3^-(aq) \rightleftharpoons :CCl_3^-* \quad K_{bind}$$

where K_a and K_{bind} are equilibrium constants, and $K_a = 10^{-25}$ because the pK_a value of $HCCl_3$ is 25. This leads to a concentration ratio of the carbenoid ($:CCl_3^-$*) and $HCCl_3$ of $[:CCl_3^-*]/[HCCl_3] = K_aK_{bind}/[H^+] = 10^{pH-25}\exp(-\Delta G_{bind}/RT)$, where ΔG_{bind} is the binding free energy of the trichlorocarbanion. The above implies that $[:CCl_3^-*]$ becomes substantial at neutral pH only when $\Delta G_{bind} < -1$ eV and exponentially increases when the pH increases. This result provides evidence that the nr-deCl pathway takes place through the formation of $:CCl_3^-$* because the higher pH produces the faster kinetics of CCl_4 decomposition observed in our experiment, which are likely due to the higher concentrations of $:CCl_3^-$* present under high pH conditions. Moreover, we note that both diss-ET pathway (Figure 4) and nr-deCl pathway (Figure 5; details will be discussed in below) requires anion exchange steps, suggesting another possible pH effect; the higher pH leads to the faster anion exchange of the surface adsorbed Cl^-* into OH^-*, promoting the CCl_4 decomposition kinetics. This explains the experimentally observed pH dependence of the reaction kinetics; (1) the formation kinetics of Cl^- was significantly enhanced at the pH regime of 5−7, which is understandable as the outcome of enhanced kinetics of the surface anion exchange considering that the low point of zero charge (PZC) value of vivianite surface that is 3.3;[34] (2) the formation kinetics of formate was significantly enhanced at the high pH regime of 11, which is understandable as the outcome of the equilibrium shift toward the carbenoid formation. We note that the two distinct pH effect promoting the surface anion exchange and carbenoid formation are advantageous in elevating the CCl_4 decomposition kinetics, and thus the kink behavior observed in the CCl_4 decomposition kinetics at the pH regime of 7−9 is conceived to be manifested by the interplay of two distinct pH effects.

To provide the full atomistic and energetic details of the reaction, we computed the DFT energetics for the nr-deCl pathway starting from $:CCl_3^-$*, as shown in Figure 5a. The water desorption energy from the Fe^{III} center where the carbenoid is located was calculated to be 0.11 eV uphill. We then found that $^-:CCl_3$* can decompose into dichlorocarbene ($:CCl_2$*) and Cl^-* at the Fe^{III} center, for which the DFT energy is only 0.07 eV uphill. This step is followed by the ligand exchange of Cl^- with OH^-, which was calculated to be 0.50 eV downhill.

We found that the Cl−C−Cl angle of $:CCl_2$* is 109.6°, which is nearly identical to the angle of free Cl−C$^{\bullet}$−Cl (110.0°) (Figure S3). Considering that CCl_2 has a trigonal planar structure with sp^2 hybridized bonds and little steric hindrance, as a following step we examined the substitution of Cl by OH, which occurs though the nucleophilic attack of OH^-* on the sp^2 carbon center of $:CCl_2$*. This yields Fe^{III} coordinated with CCl(OH) via the formation of an intermediate state of $:CCl_2(OH)^-$*. The overall change in energy for this process was calculated by DFT to be 1.31 (=0.97 + 0.34) eV downhill. By redistributing electrons and chemical bonds, CClOH* can form CO* with the release of HCl (1.17 eV downhill), which is followed by the release of CO (0.003 eV uphill).

If one additional nucleophilic attack by OH^-* on the sp^2 carbon center of :CCl(OH)* occurs, $:C(OH)_2$* will be generated via the formation of $:CCl(OH)_2^-$*, for which the overall DFT-calculated change in energy is 1.48 (1.47 + 0.01) eV downhill. The $:C(OH)_2$* can then desorb from the surface, after which proton rearrangement will occur almost immediately within the aqueous medium, yielding HCOOH. The energy required for this process was calculated to be 1.64 eV downhill.

Our DFT study of the energetics shows that the thermodynamic driving force toward the formic acid formation pathway is greater than that of the CO formation pathway (see Figure 5b), which partly explains the propensity for formation of the experimentally observed products (formate production is preferred over CO production on the vivianite surface). However, considering that both pathways are energetically available and consist of downhill processes, it is difficult to find a reasonable rationale for the CO production pathway being virtually switched-off, as was observed in our experiment. We note that the pathways discussed herein are solely based on relative thermodynamic energies; therefore, there could be additional barriers and local minima between neighboring ground states. In particular, we expect that the heterogeneous dissociation of the C−Cl bond, which is required to release HCl from CClOH* to form CO, would be kinetically unfavored. Moreover, other chemical constituents such as ions in the buffer solution or impurities may help stabilize/destabilize one pathway over the other, implying that determination of the reaction pathways could be complicated by other factors. For instance, we note that more CO was formed when we used the biogenic vivianite[3] than the chemogenic vivianite, even under the same pH conditions.

IV. CONCLUSION

Because a variety of ferrous iron minerals are known to be electron donors for CCl_4 degradation,[30,31,35−37] a thermodynamic and kinetic investigation of the reaction mechanism of the reductive dechlorination of CCl_4 by vivianite was carried out in this study. The experimental and the theoretical results represent a comprehensive investigation on the kinetics and reactive pathways of abiotic CCl_4 degradation on the surface of vivianite under anaerobic condition. These results indicate that (1) $^{\bullet}CCl_3$ is the key intermediate in the production of $HCCl_3$

DOI: 10.1021/acs.jpca.5b01885
J. Phys. Chem. A 2015, 119, 5714−5722

and formate; (2) $^{\bullet}CCl_3$ abstracts a hydrogen from surface water molecules to generate $HCCl_3$ (hydrogenolysis pathway); (3) $:CCl_3^{-}$* is formed on the vivianite surface by further reduction of $^{\bullet}CCl_3$, which also can form $HCCl_3$ when it is desorbed and protonated (carbene hydrolysis via carbenoid formation pathway); (4) $:CCl_3^{-}$* is nonreductively dechlorinated to form $:CCl_2$*, followed by sequential nucleophilic attack by OH^{-}* yielding :CCl(OH)* and $:C(OH)_2$*; and (5) :CCl(OH)* and $:C(OH)_2$* can respectively form CO and formate when they are desorbed.

The study of the CCl_4 reduction pathway on vivianite provides us with significant understanding by analyzing every reduction step. On the basis of the results of the calculated rate constants, which increase with increasing pH, the surrounding pH environment may act as an important rate-determining factor during the remediation process. According to previous studies, vivianite-rich layers formed by precipitation[44] and biotic interaction[45] are distributed in phosphorus-enriched sediments in lakes[46] and in groundwater sediments[47] where CCl_4 is detected often.[48] Therefore, the results obtained from this study indicate that the natural attenuation of CCl_4 by reductive dechlorination in the presence of vivianite at subsurfaces may be taking place.

Most studies have provided explanations for reaction mechanisms and pathways using experimental results obtained from partial transformation products, and have carried out analyses that rely on a wide variety of assumptions.[30,38] In contrast, theoretical results from DFT calculations directly suggest thermodynamically favorable intermediates on mineral surfaces for every single step, and provide a wealth of information on their molecular structures, bonding character, and oxidation states. Recently, large reaction mechanistic studies have been undertaken using computational calculations regarding sorption,[18] reductive dechlorination,[49] and oxidative decomposition,[50] among others.[15,51,52] We believe that the systematic investigation of the reaction of dechlorination taking place on a vivianite surface presented in this study may provide fundamental aid for the development of an adaptable application for other halogenated species and minerals. We believe that modeling systems and reaction mechanisms on the surfaces of structures serves not only as a supplement for experimental data but also can provide basic knowledge and optimal results through simple control of the studied environments, leading to promising alternative approaches.

■ ASSOCIATED CONTENT

Supporting Information

Computational and experimental results. The Supporting Information is available free of charge on the ACS Publications website at DOI: 10.1021/acs.jpca.5b01885.

■ AUTHOR INFORMATION

Corresponding Authors

*(H.K.) E-mail: linus16@kaist.ac.kr.
*(W.L.) E-mail: woojin_lee@kaist.ac.kr.

Author Contributions

⊥These authors contributed equally to this work.

Notes

The authors declare no competing financial interest.

■ ACKNOWLEDGMENTS

This research was supported by the Integrated Water Technology (IWT) Project (2012M1A2A2026588) funded by the Ministry of Education, Science and Technology through the National Research Foundation of Korea, and by the Global Frontier R&D Program (2013M3A6B1078884) on Center for Hybrid Interface Materials (HIM) funded by the Ministry of Science, ICT & Future Planning.

■ REFERENCES

(1) Doherty, R. E. A history of the production and use of carbon tetrachloride, tetrachloroethylene, trichloroethylene and 1, 1, 1-trichloroethane in the United States: Part 1-Historical background; carbon tetrachloride and tetrachloroethylene. *Environ. Forensics* **2000**, *1*, 69−81.

(2) Lee, W.; Batchelor, B. Abiotic reductive dechlorination of chlorinated ethylenes by iron-bearing soil minerals. 1. Pyrite and magnetite. *Environ. Sci. Technol.* **2002**, *36*, 5147−54.

(3) Moran, M. J.; Zogorski, J. S.; Squillace, P. J. Chlorinated solvents in groundwater of the United States. *Environ. Sci. Technol.* **2007**, *41*, 74−81.

(4) Bae, S.; Lee, W. Enhanced reductive degradation of carbon tetrachloride by biogenic vivianite and Fe(II). *Geochim. Cosmochim. Acta* **2012**, *85*, 170−186.

(5) Bruckner, J.; MacKenzie, W.; Muralidhara, S.; Luthra, R.; Kyle, G.; Acosta, D. Oral toxicity of carbon tetrachioride: acute, subacute, and subchronic studies in rats. *Toxicol. Sci.* **1986**, *6*, 16−34.

(6) Lee, W.; Batchelor, B. Reductive capacity of natural reductants. *Environ. Sci. Technol.* **2003**, *37*, 535−541.

(7) Lee, W. Removal of trichloroethylene in reduced soil columns. *J. Hazard. Mater.* **2004**, *113*, 175−180.

(8) Lee, W.; Batchelor, B. Abiotic reductive dechlorination of chlorinated ethylenes by iron-bearing soil minerals. 1. Pyrite and magnetite. *Environ. Sci. Technol.* **2002**, *36*, 5147−5154.

(9) Amir, A.; Lee, W. Enhanced reductive dechlorination of tetrachloroethene during reduction of cobalamin(III) by nano-mackinawite. *J. Hazard. Mater.* **2012**, *235−236*, 359−366.

(10) Choi, J.; Choi, K.; Lee, W. Effects of transition metal and sulfide on the reductive dechlorination of carbon tetrachloride and 1,1,1-trichloroethane by FeS. *J. Hazard. Mater.* **2009**, *162*, 1151−1158.

(11) Zachara, J. M.; Fredrickson, J. K.; Smith, S. C.; Gassman, P. L. Solubilization of Fe(III) oxide-bound trace metals by a dissimilatory Fe(III) reducing bacterium. *Geochim. Cosmochim. Acta* **2001**, *65*, 75−93.

(12) Roden, E. E.; Leonardo, M. R.; Ferris, F. G. Immobilization of strontium during iron biomineralization coupled to dissimilatory hydrous ferric oxide reduction. *Geochim. Cosmochim. Acta* **2002**, *66*, 2823−2839.

(13) Thinnappan, V.; Merrifield, C.; Islam, F.; Polya, D.; Wincott, P.; Wogelius, R. A combined experimental study of vivianite and As(V) reactivity in the pH range 2−11. *Appl. Geochem.* **2008**, *23*, 3187−3204.

(14) Veeramani, H.; Alessi, D. S.; Suvorova, E. I.; Lezama-Pacheco, J. S.; Stubbs, J. E.; Sharp, J. O.; Dippon, U.; Kappler, A.; Bargar, J. R.; Bernier-Latmani, R. Products of abiotic U(VI) reduction by biogenic magnetite and vivianite. *Geochim. Cosmochim. Acta* **2011**, *75*, 2512−2528.

(15) Shin, H.; Jung, S.; Bae, S.; Lee, W.; Kim, H. Nitrite reduction mechanism on a Pd Surface. *Environ. Sci. Technol.* **2014**, *48*, 12768−12774.

(16) Lim, H.-K.; Lim, H.-D.; Park, K.-Y.; Seo, D.-H.; Gwon, H.; Hong, J.; Goddard, W. A.; Kim, H.; Kang, K. Toward a Lithium−"Air" Battery: The Effect of CO2 on the Chemistry of a Lithium−Oxygen Cell. *J. Am. Chem. Soc.* **2013**, *135*, 9733−9742.

(17) Jeon, S.; Kim, H.; Goddard, W. A.; Atwater, H. A. DFT study of water adsorption and decomposition on a Ga-rich GaP(001)(2 × 4) surface. *J. Phys. Chem. C* **2012**, *116*, 17604−17612.

DOI: 10.1021/acs.jpca.5b01885
J. Phys. Chem. A 2015, 119, 5714−5722

(18) Zhang, N.; Luo, J.; Blowers, P.; Farrell, J. Understanding trichloroethylene chemisorption to iron surfaces using density functional theory. *Environ. Sci. Technol.* **2008**, *42*, 2015−2020.
(19) Sherman, D. M.; Randall, S. R. Surface complexation of arsenic(V) to iron(III) (hydr)oxides: Structural mechanism from ab initio molecular geometries and EXAFS spectroscopy. *Geochim. Cosmochim. Acta* **2003**, *67*, 4223−4230.
(20) Martin, G. J.; Cutting, R. S.; Vaughan, D. J.; Warren, M. C. Bulk and key surface structures of hematite, magnetite, and goethite: A density functional theory study. *Am. Mineral.* **2009**, *94*, 1341−1350.
(21) Blanchard, M.; Poitrasson, F.; Meheut, M.; Lazzeri, M.; Mauri, F.; Balan, E. Iron isotope fractionation between pyrite (FeS_2), hematite (Fe_2O_3) and siderite ($FeCO_3$): A first-principles density functional theory study. *Geochim. Cosmochim. Acta* **2009**, *73*, 6565−6578.
(22) Pinto, H.; Michalkova, A.; Leszczynski, J. First-principles studies of paramagnetic vivianite $Fe_3(PO_4)_2\bullet 8H_2O$ surfaces. *J. Phys. Chem. C* **2014**, *118*, 6110−6121.
(23) Meng, X.; Qin, G.; Goddard, W. A.; Li, S.; Pan, H.; Wen, X.; Qin, Y.; Zuo, L. Theoretical understanding of enhanced photoelectrochemical catalytic activity of Sn-doped hematite: anisotropic catalysis and effects of Morin transition and Sn doping. *J. Phys. Chem. C* **2013**, *117*, 3779−3784.
(24) Liao, P.; Keith, J. A.; Carter, E. A. Water oxidation on pure and doped hematite (0001) surfaces: Prediction of Co and Ni as effective dopants for electrocatalysis. *J. Am. Chem. Soc.* **2012**, *134*, 13296−13309.
(25) Kresse, G.; Furthmuller, J. Efficient iterative schemes for ab initio total-energy calculations using a plane-wave basis set. *Phys. Rev. B* **1996**, *54*, 11169−11186.
(26) Perdew, J. P.; Burke, K.; Ernzerhof, M. Generalized gradient approximation made simple. *Phys. Rev. Lett.* **1996**, *77*, 3865−3868.
(27) Fishman, M.; Zhuang, H. L. L.; Mathew, K.; Dirschka, W.; Hennig, R. G. Accuracy of exchange-correlation functionals and effect of solvation on the surface energy of copper. *Phys. Rev. B* **2013**, *87*, 245402.
(28) Bartl, H. Water of crystallization and its hydrogen-bonded crosslinking in vivianite $Fe_3(PO_4)_2{\cdot}8H_2O$; a neutron diffraction investigation. *Fresenius' Z. Anal. Chem.* **1989**, *333*, 401−403.
(29) McCammon, C.; Burns, R. The oxidation mechanism of vivianite as studies by Mössbauer spectroscopy. *Am. Mineral.* **1980**, *65*, 361−366.
(30) Danielsen, K. M.; Hayes, K. F. pH dependence of carbon tetrachloride reductive dechlorination by magnetite. *Environ. Sci. Technol.* **2004**, *38*, 4745−4752.
(31) McCormick, M. L.; Adriaens, P. Carbon tetrachloride transformation on the surface of nanoscale biogenic magnetite particles. *Environ. Sci. Technol.* **2004**, *38*, 1045−1053.
(32) Butler, E. C.; Hayes, K. F. Effects of solution composition and pH on the reductive dechlorination of hexachloroethane by iron sulfide. *Environ. Sci. Technol.* **1998**, *32*, 1276−1284.
(33) Banwart, S.; Davies, S.; Stumm, W. The role of oxalate in accelerating the reductive dissolution of hematite (α-Fe_2O_3) by ascorbate. *Colloids Surf.* **1989**, *39*, 303−309.
(34) Luna-Zaragoza, D.; Romero-Guzmán, E. T.; Reyes-Gutiérrez, L. R. Surface and physicochemical characterization of phosphates vivianite, $Fe_2(PO_4)_3$ and hydroxyapatite, $Ca_5(PO_4)_3OH$. *J. Miner. Mater. Charact. Eng.* **2009**, *8*, 591−609.
(35) Erbs, M.; Bruun Hansen, H. C.; Olsen, C. E. Reductive dechlorination of carbon tetrachloride using iron(II) iron(III) hydroxide sulfate (green rust). *Environ. Sci. Technol.* **1999**, *33*, 307−311.
(36) Kriegman-King, M. R.; Reinhard, M. Transformation of carbon tetrachloride in the presence of sulfide, biotite, and vermiculite. *Environ. Sci. Technol.* **1992**, *26*, 2198−2206.
(37) Amonette, J. E.; Workman, D. J.; Kennedy, D. W.; Fruchter, J. S.; Gorby, Y. A. Dechlorination of carbon tetrachloride by Fe(II) associated with goethite. *Environ. Sci. Technol.* **2000**, *34*, 4606−4613.
(38) Zwank, L.; Elsner, M.; Aeberhard, A.; Schwarzenbach, R. P.; Haderlein, S. B. Carbon isotope fractionation in the reductive dehalogenation of carbon tetrachloride at iron (hydr)oxide and iron sulfide minerals. *Environ. Sci. Technol.* **2005**, *39*, 5634−5641.
(39) Glod, G.; Angst, W.; Holliger, C.; Schwarzenbach, R. P. Corrinoid-mediated reduction of tetrachloroethene, trichloroethene, and trichlorofluoroethene in homogeneous aqueous solution: Reaction kinetics and reaction mechanisms. *Environ. Sci. Technol.* **1996**, *31*, 253−260.
(40) Buschmann, J.; Angst, W.; Schwarzenbach, R. P. Iron porphyrin and cysteine mediated reduction of ten polyhalogenated methanes in homogeneous aqueous solution: Product analyses and mechanistic considerations. *Environ. Sci. Technol.* **1999**, *33*, 1015−1020.
(41) Ahr, H. J.; King, L. J.; Nastainczyk, W.; Ullrich, V. The mechanism of chloroform and carbon monoxide formation from carbon tetrachloride by microsomal cytochrome P-450. *Biochem. Pharmacol.* **1980**, *29*, 2855−2861.
(42) Ullrich, V.; Schnabel, K. Formation and binding of carbanions by cytochrome P-450 of liver microsomes. *Drug Metab. Dispos.* **1973**, *1*, 176−183.
(43) Adib, K.; Camillone Iii, N.; Fitts, J.; Rim, K.; Flynn, G.; Joyce, S.; Osgood, R., Jr CCl_4 chemistry on the magnetite selvedge of single-crystal hematite: Competitive surface reactions. *Surf. Sci.* **2002**, *497*, 127−138.
(44) Nriagu, J. O. Stability of vivianite and ion-pair formation in the system $Fe_3(PO_4)_2$-H_3PO_4-H_2O. *Geochim. Cosmochim. Acta* **1972**, *36*, 459−470.
(45) Jorand, F.; Appenzeller, B.; Abdelmoula, M.; Refait, P.; Block, J.-C.; Génin, J.-M. Assessment of vivianite formation in Shewanella putrefaciens culture. *Environ. Technol.* **2000**, *21*, 1001−1005.
(46) Manning, P. G.; Murphy, T. P.; Prepas, E. E. Intensive formation of vivianite in the bottom sediments of mesotrophic Narrow Lake, Alberta. *Can. Mineral.* **1991**, *29*, 77−85.
(47) Gschwend, P. M.; Reynolds, M. D. Monodisperse ferrous phosphate colloids in an anoxic groundwater plume. *J. Contam. Hydrol.* **1987**, *1*, 309−327.
(48) Weissflog, L.; Lange, C. A.; Pfennigsdorff, A.; Kotte, K.; Elansky, N.; Lisitzyna, L.; Putz, E.; Krueger, G. Sediments of salt lakes as a new source of volatile highly chlorinated C1/C2 hydrocarbons. *Geophys. Res. Lett.* **2005**, *32*.
(49) Nonnenberg, C.; van der Donk, W. A.; Zipse, H. Reductive dechlorination of trichloroethylene: A computational study. *J. Phys. Chem. A* **2002**, *106*, 8708−8715.
(50) Zhu, W.; Liu, X.-Q.; Hou, X.; Chen, J.; Kim, C. K.; Xu, K. Modelling in catalytically oxidative decomposition of carbon tetrachloride on ZnS nanocluster using density functional theory. *Catal. Sci. Technol.* **2014**, *4*, 1038−1046.
(51) Filippi, C.; Healy, S. B.; Kratzer, P.; Pehlke, E.; Scheffler, M. Quantum Monte Carlo calculations of H_2 dissociation on Si(001). *Phys. Rev. Lett.* **2002**, *89*, 166102.
(52) Wu, T.; Werner, H.-J.; Manthe, U. Accurate potential energy surface and quantum reaction rate calculations for the $H+CH_4 \rightarrow H_2+CH_3$ reaction. *J. Chem. Phys.* **2006**, *124*, 164307.

DOI: 10.1021/acs.jpca.5b01885
J. Phys. Chem. A 2015, 119, 5714−5722